Cite as: Efthymiou E and Camara A (2021). Inelastic response of cable-stayed bridges subjected to non-uniform motions. Bulletin of Earthquake Engineering. Currently in press.

Inelastic response of cable-stayed bridges subjected to non-uniform motions

Eleftheria Efthymiou · Alfredo Camara

Received: date / Accepted: date

Abstract This paper studies for the first time the effect of the Spatial Variability of Ground Motions (SVGM) with large intensities on the inelastic seismic response of the pylons which are responsible for the overall structural integrity of cable-stayed bridges. The SVGM is defined by the time delay of the earthquake at different supports, the loss of coherency of the seismic waves and the incidence angle of the ground motion. An extensive study is conducted on cable-stayed bridges with 'H'- and inverted 'Y'-shaped pylons and with main spans of 200, 400 and 600 m. The SVGM is most detrimental to the pylon of the 200-m span bridge owing to the large stiffness of this bridge compared to its longer counterparts. The stiff configuration of the inverted 'Y'-shaped pylon makes it more susceptible against the multi-support excitation than the flexible 'H'-shaped pylon, especially in the transverse direction of the response. Finally, the earthquake incidence angle is strongly linked with the SVGM and should be included in the seismic design of cable-stayed bridges.

Keywords spatial variability · cable-stayed bridges · pylon · incidence angle · non-linear dynamic analysis · incoherence effect · wave-passage effect

1 Introduction

The Spatial Variability of the Ground Motion (SVGM) also referred to as multi-support excitation is described by the differential movement of the supports of long structures. It is present when a structure is long with respect

Eleftheria Efthymiou
Department of Civil and Environmental Engineering, Lyle School of Engineering, Southern Methodist University, Dallas, TX, USA
Tel.: +1 (214) 768-3894
E-mail: eefthymiou@smu.edu

Alfredo Camara
School of Mathematics, Computer Science and Engineering, City University of London, London, UK

to the wavelength of the input motion in the frequency range of importance to the response of the structure. As a result, its supports may be subjected to different excitations [3] and this is known to affect the structural response depending on the amplitude of the seismic motion, the incidence angle of the earthquake relatively to the the structure, the geometric characteristics of the structure and the stiffness of the surrounding soil among others [30,35,26,4, 51,45,46,49,5,42,47,39,43,33].

The SVGM results from the combination of four effects [14,13]; the wave-passage effect which refers to the difference in the arrival times of the ground motion at different supports; the incoherence effect which refers to the loss of coherency of the ground motion due to successive reflections and refractions of the seismic waves in heterogeneous soil media along their path; the site response effect which reflects the modification of the amplitudes and the frequency contents of the ground motions at different supports due to changes in the local site conditions; and the attenuation effect which describes the gradual decrease of the amplitudes of the seismic waves with distance as they travel away from the fault.

The SVGM can be detrimental on stiff structures whereas, it typically does not significantly affect the response of longer and more flexible structures [4,37]. The increased influence of the SVGM on stiff structures is due to the pseudo-static component of the structural response [40,52], as opposed to flexible structures wherein the response is dominated by the dynamic component [6]. In cable-stayed bridges that are composed of elements with very different flexibilities, this observation can be extended in the sense that their stiffer components are more vulnerable to the multi-support excitation.

The wave-passage effect is an important component of the SVGM especially in the long spans that are usually associated with cable-stayed bridges where the time delay of the earthquake at different supports can be more important than the incoherence of the ground motion. Typically lower values of the wave propagation velocity increase the structural response by increasing the pseudo-static forces caused by the SVGM and by decreasing their dynamic counterpart [4,51,46,47,50,6]. The incoherence effect is usually more pronounced than the wave-passage effect which can be neglected when the seismic waves present a high rate of incoherence [51,45].

More recently, the earthquake incidence angle combined with the SVGM has gained the attention of the research community, with a limited number of studies stating that the maximum structural response of a cable-stayed bridge may not be obtained when the direction of propagation coincides with the principal axes of the bridge [5,32].

The aforementioned works focus on the elastic seismic response of structures under the SVGM, but there is lack of works on the inelastic response of the pylons of cable-stayed bridges under large non-uniform ground motions. It is important to understand the response of these structures under extremely large records, which could exceed the design limits. Indeed, important damages have been reported in several cable-stayed bridges after strong earthquakes in the 80's and 90's. This is the case of the Shipshaw Bridge (Canada, 183-m

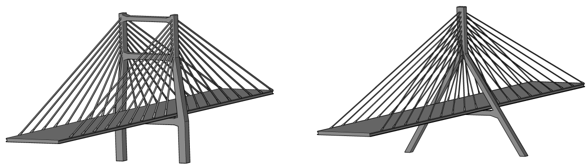

(a) H-LCP (b) Y-LCP

Fig. 1 Adopted pylon shapes and their reference keywords. The part of the notation before the hyphen reflects the shape of the pylon; whereas the part after the hyphen characterises the cable arrangement. In this work the deck is supported on two lateral cable planes (LCP).

span), damaged at the connection between the deck and the pylon during the 1988 Saguenay earthquake, with moment magnitude $M_W = 6.0$ [24]. In addition, the piers of the Higashi–Kobe Bridge (Japan, 485-m span) were also damaged during the Hyogo-Ken Earthquake [7]. But perhaps the most significant seismic damage was caused by the 1999 Chi-Chi Earthquake at the pylon of the Chi–Lu Bridge (Taiwan, 120-m span) [11]. Even though these partial failures are deemed inadmissible today, the large social and economic importance of cable–stayed bridges, which emphasizes the need for research on this topic. This paper focuses on the effect of the SVGM and the incidence angle of the earthquake on the inelastic seismic response of the pylons of cable-stayed bridges with different structural configurations and dimensions. Important conclusions are reached through the comparison between the elastic and the inelastic seismic responses of the bridges. The effect of the SVGM on the pylons with variable heights is investigated and the role of the pylon shape as a means to resist the SVGM is also thoroughly discussed. The influence of the multi-support excitation on the seismic response of the pylons is strongly affected by the shape of the pylons, their overall dimensions, the part of the pylon under examination and by the earthquake incidence angle.

2 Modelling and Analysis

2.1 Numerical Models

The bridge models employed in this study are based on the work of Camara *et al.* [9] and Efthymiou [15]. The overall bridge arrangement consists of two symmetric reinforced concrete pylons, a composite deck and the cable system. The length of the main span, L_P, is equal to 200, 400 and 600 m, representing short-span, intermediate-span and relatively long-span cable-stayed bridges, respectively. Pylons with conventional 'H' and inverted 'Y' shapes have been considered, as shown in Fig. 1 wherein the notation of the pylons is also included and will be followed hereinafter.

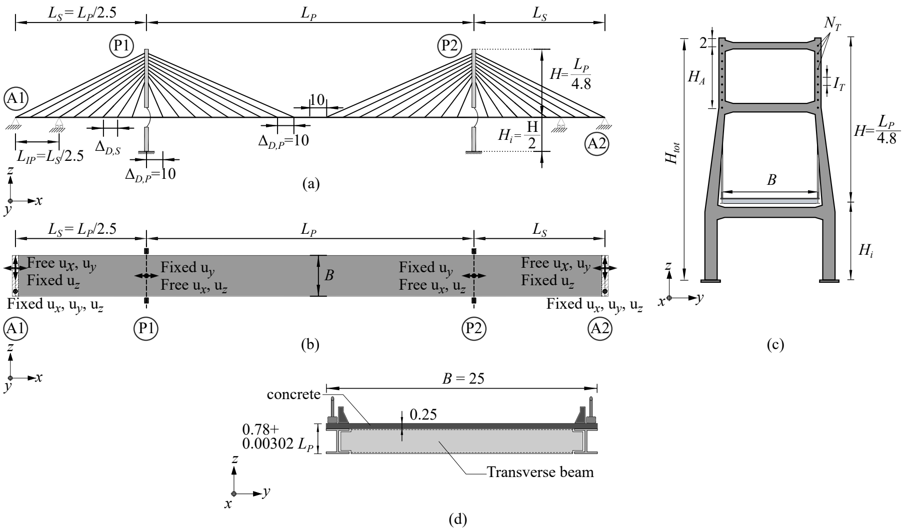

Fig. 2 Parametric definition of the cable-stayed bridges. (a) Elevation, (b) Plan view, (c) sample pylon (the same parametrisation rules are applied to the 'H' and the inverted 'Y'-shaped pylons), (d) deck. All dimensions are in [m].

The length of the side spans, L_S, is described by L_P as shown in Fig. 2. L_P also defines the number of cables, N_T, in each plane; $N_T = 9$, 19 and 29 when $L_P = 200$, 400 and 600 m, respectively. The height of the pylons above the deck level is $H = {}^{L_P}\!/_{4.8}$ in both pylon configurations. The height of the pylons below the deck is $H_i = {}^{H}\!/_{2}$, resulting in the total height of the pylons: $H_{tot} = H + H_i = 62.5$, 125 and 187.5 m for the 200-, 400- and 600-m main span bridges, respectively. The dimensions of the different members of the pylons and of the various cross sections are functions of H [9].

The cables form a semi-harp configuration in the direction parallel to the traffic. Two lateral cable planes (LCP) hold the 25-m wide deck that accommodates four traffic lanes, regardless of the length of the bridge. The deck has an open composite cross-section formed of two longitudinal I-shaped steel girders at the edges and a 25-cm thick concrete slab on top. The overall stability of the deck is provided by transverse I-beams located at fixed intervals (≈ 5 m apart) that connect the two longitudinal girders. In the side spans intermediate piers at a distance of L_{IP} from the abutments constrain the vertical displacement of the deck and consequently control the longitudinal displacement of the upper part of the pylon (see Fig. 2).

The abutments constrain the movement of the deck in the vertical (z), transverse (y) and longitudinal ($x /\!/$ traffic) directions and they also prevent its torsional rotation (θ_{xx}) as shown in Fig. 2(b). The movement of the deck is constrained in the three orthogonal directions with POT bearings at the edges of the deck. The torsional rotation is prevented due to the eccentricity of the POT supports that constrain the vertical movement of the deck relative to its centerline. The model of these support devices does not account for their flexibility, i.e. they are modelled as fully-fixed eccentric points linked to the beam element representing the deck at its centroid. This is deemed admissible given the large stiffness of POT devices in the direction in which they restrain the displacement, and the small effect that including their flexibility (e.g. with spring elements) would have in the overall seismic response of the bridge. The piers at the side spans constrain the vertical displacement and the torsional rotation of the deck. At the pylons, the deck is only restrained in the y direction assuming a floating connection between the deck and the pylon — a common solution in the design of cable-stayed bridges in seismic prone regions.

The soil–structure interaction has been considered by applying systems of springs and dashpots at the base of the pylons. The dynamic impedances are computed for the movement in the three principal directions of the bridge and for the rotation around the x and y axes. The spring and dashpot systems have constant properties that are obtained from the work of Gazetas [25] and are calibrated to the mean frequency of the earthquakes, f_m [48], as:

$$f_m = \frac{\sum_i C_i^2}{\sum_i C_i^2 \left(\frac{1}{f_i}\right)} \tag{1}$$

where C_i are the Fourier amplitude coefficients and f_i are the discrete fast Fourier transform (FFT) frequencies between 0.20 Hz $\leq f_i \leq$ 20 Hz.

The constituent materials (steel and concrete) of the cable-stayed bridges are described through their constitutive models and their properties are defined in the relevant Eurocodes [19–21,23]. The concrete in the pylons is C40 concrete with characteristic strength of $f_{ck} = 40$ MPa [19] and it is confined with transverse reinforcement bars following the model of Mander *et al.* [36]. To ensure adequate concrete confinement longitudinal and transverse reinforcement ratios of 2.4% and 0.8%, respectively are considered in the pylons [1,38]. B500C steel grade is used for the deck and for the reinforcement with yield stress of 552 MPa. The prestressing steel forming the cables has a Young's modulus of $E_p = 190$ GPa. In this work the nonlinear material behaviour is only considered in the pylons, which appeared to be the most vulnerable elements in cable-stayed bridges subjected to large ground motions [11], whereas the concrete slab, the steel members of the deck and the cables behave elastically. The structural damping in the dynamic analysis follows a Rayleigh's damping distribution with a maximum damping ratio of 2% to account for the small structural dissipation in cable-stayed bridges [31] and it is independent of the material (concrete or steel). The range of important frequencies for the structural response of the examined bridges is defined at the lower bound by the fundamental frequency (f_1) of the bridges. f_1 is equal to 0.49, 0.33 and 0.20 Hz for the 200, 400 and 600-m span bridges, respectively and it is almost insensitive to the pylon shape and to the type of cable system. The upper bound of the important frequency range is set as 20 Hz in all cases [8].

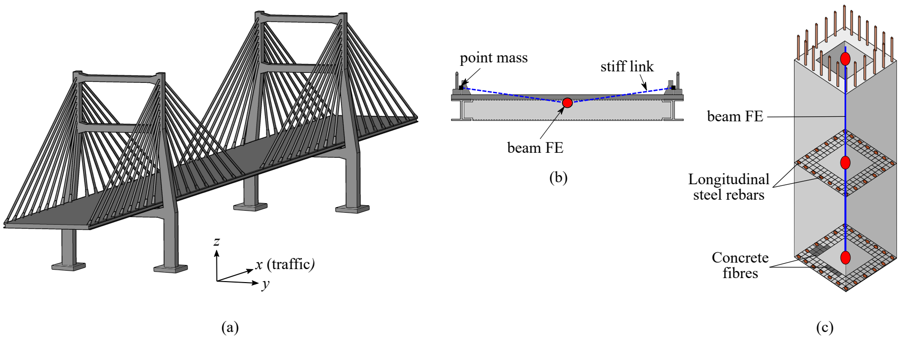

Fig. 3 (a) Complete 3D model of the H-LCP bridge with $L_P = 200$ m, (b) FE model of the LCP deck and (c) FE model of the pylon.

The finite element (FE) analysis software Abaqus [2] has been used to model the bridges and to conduct the complete sets of dynamic analyses. Figure 3 shows that the deck sections are discretised with linear interpolation shear-flexible beam-type elements that pass through the centre of gravity of the deck sections and account for the structural (reinforced concrete slab, longitudinal and transverse steel girders and steel diaphragms) and nonstructural (deck asphalt) masses, as shown in Fig. 3(b). Lump mass elements located at both cable ends represent the anchorage masses which, at the deck end of each cable, also include the parapets. The pylons are modelled with fibre beam elements through the centre of gravity of their sections. The nonlinear cyclic degradation of the confined concrete is defined through the smeared crack concrete model. Finally, the cables are modelled with 3D trusses which use linear interpolation of the axial displacements. Each truss element represents one cable, ignoring the cable-structure interaction [16].

2.2 Seismic Action

Seven sets of artificial accelerograms have been generated based on the response spectrum of Eurocode 8 [22] with 2% damping, $a_g = 0.5g$ and for ground category D, which represents soft soil conditions. Each set consists of four bi-directional accelerograms that are generated for each of the supports of the bridges with horizontal restraints (i.e. the two abutments and the two pylons). This means that the two horizontal components of the seismic action have been considered — namely 'Fault Parallel' (FP) and 'Fault Normal' (FN), the latter coinciding with the direction of wave propagation. Artificial accelerograms are not associated to principal components in their generation process, hence an intensity ratio between the major and minor earthquake components has been adopted to account for the observed differences in the propagation of the waves in the directions perpendicular and parallel with respect to the fault. To this end, for the FP component the response spectrum is reduced to 70% of the original FN component [34].

The resulting accelerograms have been modified by the empirical coherency model of Harichandran and Vanmarcke [27] to account for the loss of coherency among the accelerograms at the different supports of the bridges. Following the consideration of several empirical and semi-empirical coherency models [17], the adopted model of Harichandran and Vanmarcke [27] has been deemed the most appropriate for this work because it considers incoherent seismic waves even in low frequencies, which are of importance to the response of cable-stayed bridges. The coherency is assumed independent of the direction of propagation allowing for the same coherency model to be used for the generation of signals in the FN and FP directions [44].

The temporal variability of the ground motion (i.e. the wave-passage effect) is also accounted for by means of the delay in the arrival of the earthquakes at neighbouring supports. The first abutment (A1) is affected by the earthquake at time instance $t_{\mathrm{A1}} = 0$ s and then the ground motion travels parallel to the deck with propagation velocity $c = 1000$ m/s reaching the first pylon (P1), the second pylon (P2) and the second abutment (A2). The time delay between pylons P1 and P2 reaches 0.2, 0.4 and 0.6 s in the bridges with $L_P = 200$, 400 and 600 m.

The generation of the spectrum-compatible acceleration histories follows the iterative scheme proposed by Deodatis [12]. In this methodology, at the end of the i^{th} iteration the accelereration history, $\ddot{u}^{(i)}_{g,\,j}(t)$, is obtained for each support j and the response spectrum of $\ddot{u}^{(i)}_{g,\,j}(t)$, $\mathrm{RS}^{(i)}_j$, is compared to the target $\mathrm{RS}^{\mathrm{target}}_j$ and the process is repeated with an updated S_{jj} until acceptable convergence is reached, as follows:

$$S^{(i+1)}_{jj}(\omega) = \left[\frac{\mathrm{RS}^{\mathrm{target}}_j(\omega)}{\mathrm{RS}^{(i)}_j(\omega)}\right]^2 S^{(i)}_{jj}(\omega) \tag{2}$$

where: S_{jj} is the power spectral density at station j for the previous (i^{th}) and the next ($i^{\mathrm{th}} + 1$) iterations. More details about the generation of spectrum-compatible accelerograms that account for the SVGM are included in [15]. In this work, the iterations stop when the response spectra of the individual accelerograms fall within the range 90%-110% of the target spectrum in the range of important periods of the studied bridges: $[0.2T_1,\ 1.2T_1]$; T_1 being the fundamental vibration period of the structure in each case [8]. For the two different structural typologies, T_1 is 2.03, 3.02 and 5.01 s on average when $L_P = 200$, 400 and 600 m, respectively. The accelerograms are then baseline-corrected to ensure there are no residual displacements at the end of the time-histories. An indicative set of accelerograms corresponding to the FN component for the supports of the 400-m main span bridge is included in Fig. 4(a), where the time delay and the loss of coherency can be appreciated. Figure 4(b) shows a good match between the FN and FP target spectra and those of the resulting signals.

Two different orientations of the bridges have been examined aiming to address the effect of the angle of incidence, θ, of the earthquake. In the first

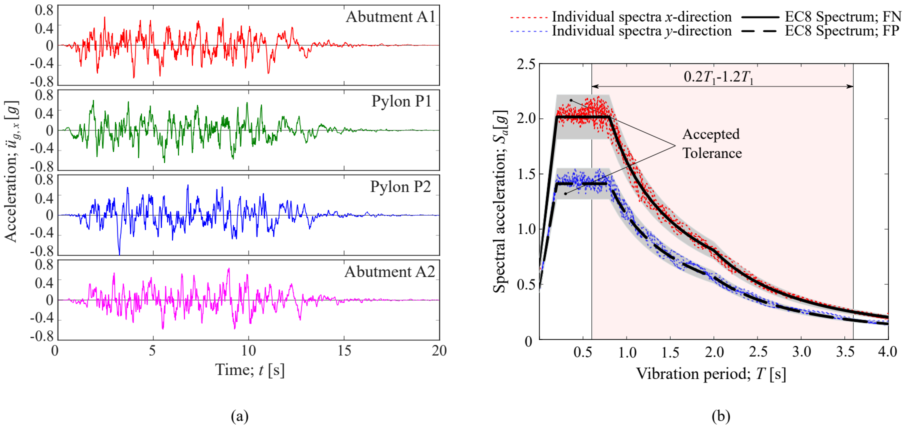

Fig. 4 (a) Indicative set of accelerarograms when c = 1000 m/s, (b) individual response spectra from the generated accelerograms. The target response spectra are also included. L_P = 400 m.

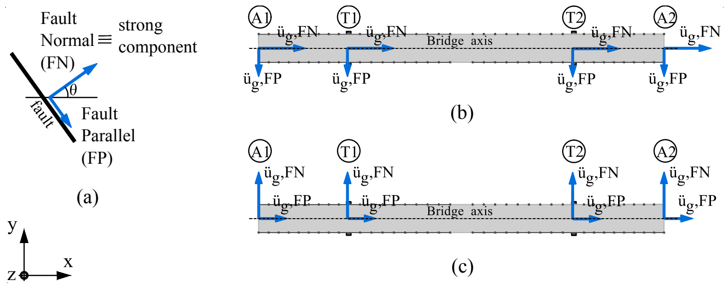

Fig. 5 Schematic representation of the angle of incidence (θ) of the seismic waves with respect to the bridges. (a) Principal earthquake components; (b) $\theta = 0°$ and (c) $\theta = 90°$.

case (namely $\theta = 0°$) the FN component, which represents the strong earthquake component, propagates parallel to the bridge and the FP (i.e. 0.7FN) component acts perpendicular to the bridge. In the second case ($\theta = 90°$) the bridge is rotated by 90° clockwise, making the FN component act transversely with respect to the bridge, as shown in Fig. 5.

The wave-passage and incoherence effects are dependent on the orientation of the bridge with respect to the ground motion. The travelling distance of the seismic waves, r_{ij} with i, j = A1, P1, P2 and A2 and $i \neq j$, is a function of the distance between supports, L_{ij}, and of θ, as: $r_{ij} = L_{ij} \cos\theta$. As a result, when $\theta = 0°$ both the time delay and the loss of coherency between supports are maximised. On the other hand, when $\theta = 90°$ the seismic waves are considered completely coherent and the time delay is zero, reducing essentially the problem to the identical support motion.

2.3 Methodology

Elastic and inelastic dynamic analyses have been performed to evaluate the seismic behaviour of the cable-stayed bridges. The geometric nonlinearities that arise from large deformations, which are inherent in cable-stayed bridges [4], have been accounted for both in the elastic and the inelastic analyses of the bridges. The system of dynamics is integrated step-by-step during the analysis. The direct implicit HHT algorithm [29] is used in the nonlinear analysis of the bridges with $\alpha = -0.05$ in order to reduce the high frequency noise that is introduced to the integration with every time step [2]. The time step for the integration is selected from a sensitivity analysis as $\Delta t = 0.01$ s, which is the same as that of the accelerograms, but can be reduced down to $\Delta t = 10^{-5}$ s so that numerical convergence is reached.

The effect of the SVGM on the seismic response of the pylons is evaluated by means of the peak seismic axial load (N), the longitudinal (V_x) and the transverse (V_y) shear forces along the pylon legs. The deformations of the concrete and the steel reinforcement (ε_{tot}) in the pylons are also examined. The results are obtained for the second pylon that receives the SVGM (P2) because its effect on this pylon has been found more important than on P1 in previous studies on the elastic seismic response of cable-stayed bridges [18]. In fact, the apparent symmetry of the structures described in Section 2.1 of the manuscript is lost in the seismic response for different incidence angles (θ) due to: (1) the longitudinal movement of the deck during the earthquake, which introduces axial compression in one pylon and tension in the opposite due to the effect of the cable system; (2) the difference in the ground motion at different supports due to the loss of coherency and the time lag from the SVGM (Fig. 4(a)); and (3) the lack of symmetry of the support conditions at the abutments A1 and A2 with respect to the centreline of the deck (axis x), as shown in Fig. 2(b). The asymmetry of the response that is observed both in the SVGM and the SYNC motion is mainly relevant in the longitudinal direction. This is attributed to the effect of the cable system transferring the longitudinal shear forces from one pylon to the opposite. This effect increases with the restraint of the cable system to the relative (out-of-phase) longitudinal movement between the pylons. In the transverse direction of the response the pylons remain relatively unconstrained from the cable system and the deck (floating deck–pylon connection), and as a result the difference between the transverse response of the two pylons is negligible. The results are obtained in the form of time-histories of the forces and strains from the individual earthquakes at the different regions of the legs and subsequently, the peak (maximum absolute) values are identified. For the forces, the effect of the self-weight is subtracted from the time-histories in order to focus solely on the seismic response. For the deformations of the concrete and the steel reinforcement, the strain induced by the self-weight prior to the seismic action is also considered. The deformations are examined at the corner of the concrete sections of the pylons, where the maximum strains are recorded, and also at the corner reinforcement bars, as can be seen in Fig. 6. The positive values

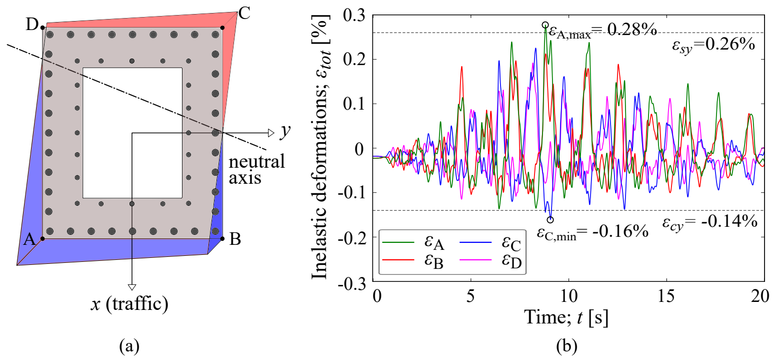

Fig. 6 (a) Schematic representation of the strain distribution in a typical section of the pylon and (b) Time-histories of the deformation at the corners of the section; H-LCP model; L_P = 200 m; $\theta = 0°$; seismic record #7; SYNC motion.

of the deformations (ε^+) denote tension and the negative values (ε^-) denote compression. The cracking in the concrete sections is considered to be excessive when the steel reinforcement yields in tension ($\varepsilon_s \geq \varepsilon_{sy} = 0.26\%$) which is associated with slight-to-moderate concrete cracking [28], whereas the compressive deformation demand in the concrete is considered inadmissible when the peak compressive elastic limit $\varepsilon_{cy} = f_{cm}/E_c = 0.14\%$ is exceeded, and the concrete crushes in compression.

Eventually, the results are presented in terms of the arithmetic average of the peak seismic forces and the deformations of the materials (μ) from the performed dynamic analyses R_i (with $i = 1 \rightarrow 7$ denoting the sets of accelerograms applied). In this work the dispersion of the individual seismic responses is also considered in terms of the standard deviation (±SD) from the mean peak seismic response (μ_{SYNC}) obtained from the reference synchronous (SYNC) motion of the supports.

The increments in the seismic response due to the SVGM are quantified by the ratio ρ of the seismic response from the SVGM over the respective response from the SYNC motion:

$$\rho_j = \frac{\mu_{\text{SVGM},j}}{\mu_{\text{SYNC},j}} \tag{3}$$

where $\mu_{i,j}$ with i = SVGM, SYNC is the arithmetic mean (from the seven sets of accelerograms) of the peak response: $j = N$, V_x, V_y, ε_{tot}.

3 Influence of the SVGM on the Seismic Response of the Pylons

3.1 Effect of the Material Nonlinearity

Figure 7 shows that the material nonlinearities reduce the seismic-induced V_x (Fig. 7(a)) and V_y (Fig. 7(b)) in the bridge with L_P = 400 m, compared to their respective magnitudes when the materials (concrete and renforement steel) have linear elastic behaviour. This reduction is attributed to the plastic

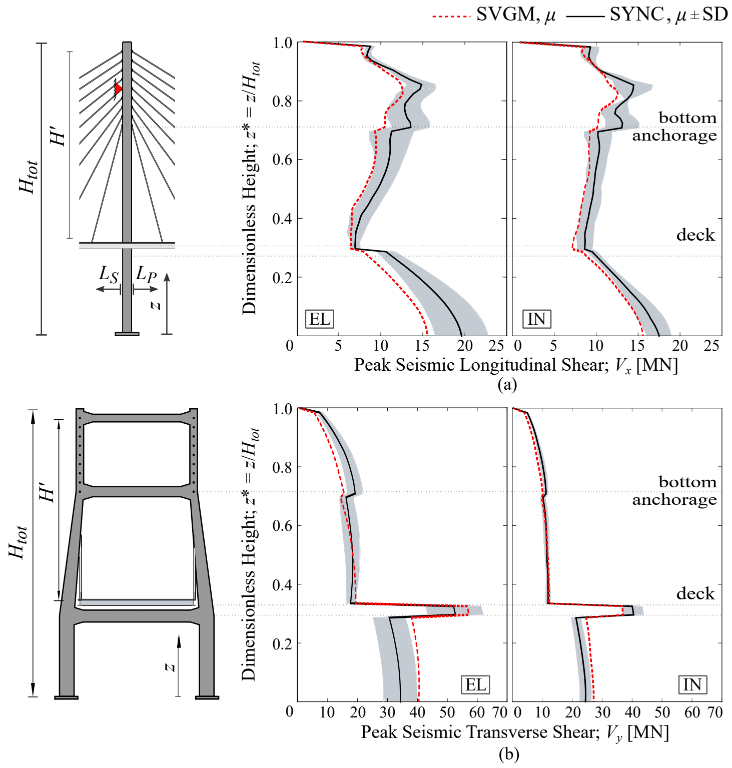

Fig. 7 Peak elastic (left) and inelastic (right) seismic response in pylon P2. (a) V_x and (b) V_y. H-LCP bridge; $L_P = 400$ m; $\theta = 0°$ (i.e. FN // traffic).

dissipation of the input seismic energy that provides an additional damping mechanism in the pylons. Focusing on the SYNC motion first, the longitudinal seismci shear force, $V_{x,\mathrm{IN}}$, is reduced by 10% at the base of the pylon compared to $V_{x,\mathrm{EL}}$ and $V_{y,\mathrm{IN}}$ is reduced by 25% from $V_{y,\mathrm{EL}}$ at the area between the deck and the lower strut when material nonlinearities are considered. The larger reduction in V_y is associated with the transverse reaction that the deck exerts to the pylon, which is dominated by the fundamental transverse vibration mode of this bridge [10]. Looking at the response from the SVGM, the reduction in V_x at the base of the pylon when material nonlinearities are considered is negligible, which suggests that there is no plastic dissipation at this region of the pylon from the longitudinal out-of-phase motion of the pylons. On the other hand, the transverse shear force, $V_{y,\mathrm{IN}}$, from the SVGM is reduced by 47% compared to $V_{x,\mathrm{EL}}$ at the deck level, indicating that in this direction there is damage from the plastic dissipation of the seismic energy in the pylon, from the deck level down to the foundation.

The results of the elastic and inelastic analyses of the cable-stayed bridge in Fig. 7(a) demonstrate that the SVGM consistently results in smaller V_x than the SYNC motion along the height of the pylon, implying that the multi-support excitation is not important in the longitudinal response of the pylon. Figure 7(b) shows that when the material nonlinearities in the pylon are considered the transverse response above the deck from the SVGM resembles the seismic SYNC response. This is because the transverse out-of-phase oscillation of the two pylons is not significantly restrained by the cable-system. On the other hand, the SVGM reduces the inelastic V_y at the deck level of the pylon compared to the SYNC motion, but increases the elastic V_y. This is because in this region of the pylon the SVGM results in larger damage than considering the SYNC ground motion. The results from Fig. 7 indicate that the SVGM is more detrimental for the transverse response of the pylon than it is for the longitudinal response because in the former case the reduction of the peak shear force demand is greater than that from the SYNC motion. This important observation suggests that the effect of the longitudinal restraint of the cable-system to asynchronous motions is less important than the increased transverse deck–pylon reaction under the SVGM.

3.2 Effect of the Incidence Angle of the Ground Motion

The influence of the earthquake incidence angle is explored by comparing the seismic responses of the intermediate-span bridge when the FN earthquake component is parallel (i.e. when $\theta = 0°$) and perpendicular ($\theta = 90°$) to the traffic. The results are presented in Fig. 8 which shows that the longitudinal shear force, V_x, is larger when $\theta = 0°$ than that when $\theta = 90°$ for the SYNC motion and for the SVGM. Accordingly, the transverse shear force, V_y, when $\theta = 90°$ is larger than the obtained response when $\theta = 0°$ for the SYNC motion as well as for the SVGM. The differences in the response between the two orientations is related to the FP earthquake component being 70% of the FN component. Specifically, Fig. 8 shows that $V_{x\ \mathrm{IN,SYNC}}$ at the base of the pylon is reduced by 25% when $\theta = 90°$ compared to the responses obtained when $\theta = 0°$. On the other hand, the transverse shear, $V_{y\ \mathrm{IN,SYNC}}$ at the deck-pylon connection level is increased by 15%. This shows that the seismic response in each direction is maximised when the strong earthquake component is applied parallel to this direction. The axial load at the base of the pylon is not affected by the different orientations of the bridge in the SYNC motion case. Figure 8 also demonstrates the negligible effect of the SVGM on the three directions of the seismic response when $\theta = 90°$ compared to the SYNC motion. As discussed in Section 2.2 the wave-passage and the incoherence effects are orientation dependent and hence when $\theta = 90°$ the problem is reduced to the SYNC motion of the supports.

Figure 9 presents the plastic strains along pylon P2 of the H-LCP bridge with $L_P = 400$ m when $\theta = 0°$ and 90° under the SYNC motion. The sections of the pylon that exceed the strain limits defined in Section 2.3 are highlighted with red colour. In order to distinguish between the two orientations, the plastic strains when $\theta = 0°$ are noted on the left half of the pylon and the strains when $\theta = 90°$ are included on the right half. The large plastic strains in the

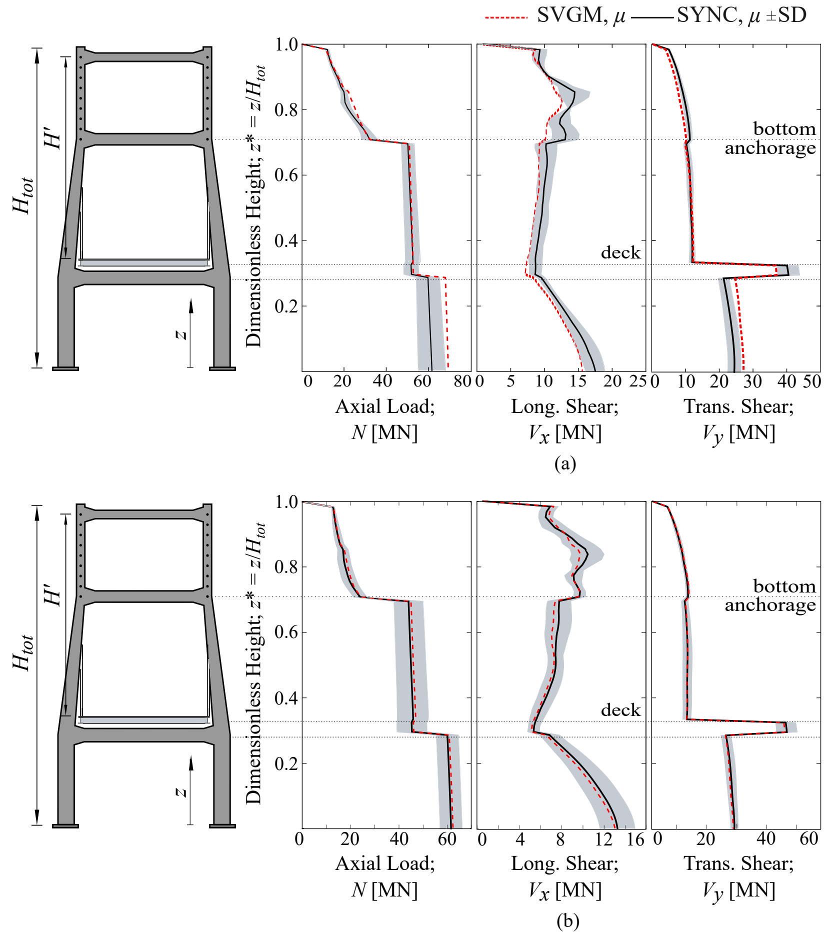

Fig. 8 Peak inelastic seismic N, V_x and V_y in pylon P2 when (a) $\theta = 0°$ and (b) $\theta = 90°$. H-LCP bridge; $L_P = 400$ m.

steel reinforcement bars suggest that the connections of the legs with the upper and the intermediate struts along with the base of the pylon are the most sensitive regions of the pylon. In these sections, the steel exceeds its yielding deformation and the concrete softens in compression. The peak tensile deformations are larger than the respective peak compressive deformations because when cracking is initiated in the concrete ($\varepsilon_{c,crack} = 0.0086\%$) the neutral axis of the section is shifted towards the compression part of the section, resulting in higher increments of the tensile deformation. The incidence angle of the earthquake influences the amount of cracking, which is larger when $\theta = 90°$, as shown in Fig. 9(b). When $\theta = 90°$ the strong earthquake component is applied parallel to the pylon struts and the relative oscillation of its lateral legs is more pronounced, which explains the 50%-increase in the inelastic deformations at the connection of the legs with the upper transverse struts compared

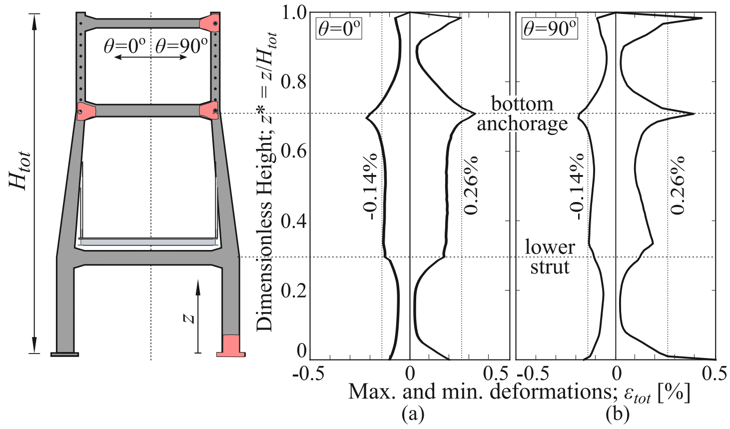

Fig. 9 Peak inelastic deformations of the concrete (compression) and the steel reinforcement (tension) in pylon P2 when (a) $\theta = 0°$ and (b) $\theta = 90°$. H-LCP, $L_P = 400$ m, SYNC ground motion. The highlighted areas in the pylon denote yielding of the materials.

to the deformations for $\theta = 0°$ in Fig. 9(a). Similarly, the plastic deformation is increased by 17% at the connection between the legs and the intermediate struts and by 150% at the base of the pylon when $\theta = 90°$.

3.3 Influence of the Pylon Shape

The peak seismic forces in the 400-m span bridges with 'H'- and inverted 'Y'-shaped pylons is compared in Fig. 10 when $\theta = 0°$. The difference in the seismic response between the two pylon configurations is initially examined in the SYNC motion. The inclined legs of the inverted 'Y'-shaped pylon connected above the deck result in an overall stiffer pylon configuration compared to the relatively flexible 'H'-shaped pylon [10], which works as a Vierendeel truss in the transverse direction. For this reason, V_y is almost double at the level of the bottom anchorage in the pylon of the Y-LCP model than the one at the same region of the 'H'-shaped pylon, and the seismic axial force, N, is 50% larger. This is associated with the reaction of the deck to the pylon legs which, due to their outward inclination, is resolved into one component perpendicular to the axis of the legs and the other parallel to it. Given the large inclination of the legs in the inverted 'Y'-shaped pylon, the component of the deck–pylon reaction that is parallel to the legs is larger than that in the 'H'-shaped pylon, which justifies the larger seismic axial force in the Y-LCP model. On the other hand, the force component perpendicular to the legs is larger in the H-LCP model due to the slight inclination of the intermediate part of the legs in this type of pylons. This explains the 30% increase in V_y at the deck level of the H-LPC model compared to the Y-LCP model.

The top vertical member of the pylon of the Y-LCP bridge differentiates the effect of the SVGM from that obtained in the individual legs of the 'H'-

shaped pylon. The SVGM increases N by a maximum of 40% compared to the SYNC motion at the anchorage area of the pylon with inverted 'Y' shape, which indicates that the SVGM affects more this bridge than the one with 'H'-shaped pylons. More specifically, in the anchorage area of the pylon of the Y-LCP bridge $\rho_{N,\text{Y-LCP}} = 1.41$ whereas $\rho_{N,\text{H-LCP}} = 1.0$ in the same area of the H-LCP model. This increment can be explained by the increased stiffness of the top part of the inverted 'Y'-shaped pylon compared to the 'H'-shaped pylon. In pylons of inverted 'Y' shape, the transverse movement of the connection between the individual legs and the top vertical member is constrained due to the inclination of the legs, resulting in a stiffer configuration than that of 'H'-shaped pylons which behave as Vierendeel beams in the transverse direction.

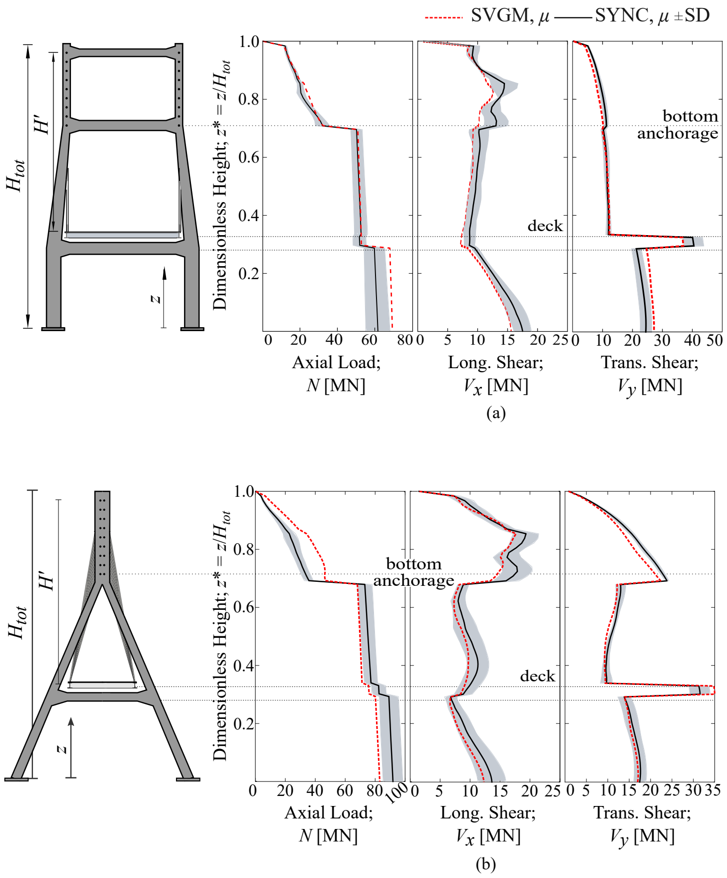

Fig. 10 Mean peak inelastic seismic seismic forces along the height of pylon P2 in the (a) H-LCP and (b) Y-LCP models. $L_P = 400$ m; $\theta = 0°$ (i.e. FN // traffic).

Despite the different geometries of the inverted 'Y'- and the 'H'-shaped pylons, the part of the pylons at the deck level in both configurations is the most affected by the SVGM because of the reaction that the deck exerts to

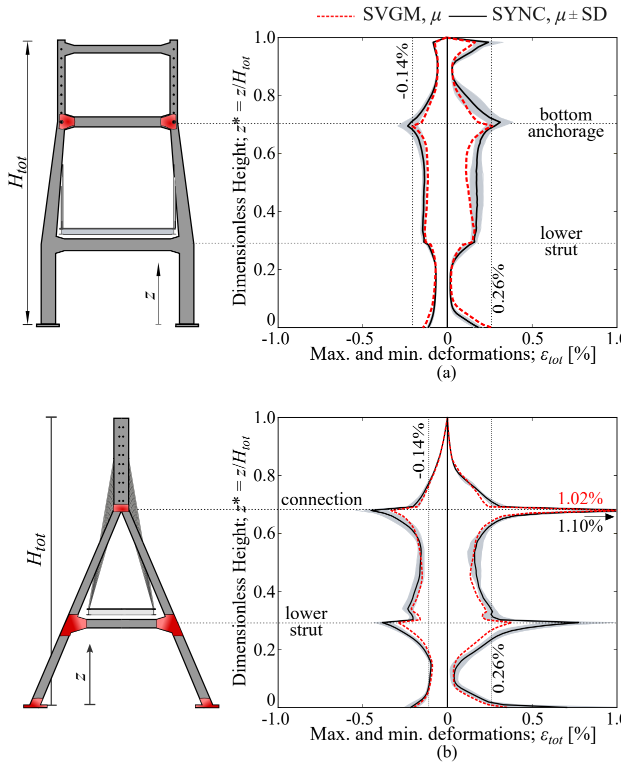

Fig. 11 Peak inelastic deformations of the concrete and the steel reinforcement in pylon P2 in the (a) H-LCP and (b) Y-LCP models. $L_P = 400$ m, $\theta = 0°$.

the pylons. In the Y-LCP model $\rho_{V_y,\text{Y-LCP}} = 1.09$ whereas in the 'H'-shaped pylon $\rho_{V_y,\text{H-LCP}} = 0.92$ at the level of the deck–pylon connection. The transverse response ratios suggest that the stiffer transverse configuration of the inverted 'Y'-shaped pylon makes it less capable to accommodate effectively the multi-support excitation than the more flexible 'H'-shaped pylon. In the longitudinal direction of the response (V_x), the SVGM reduces the seismic response of both pylon configurations from the SYNC excitation regardless of their shape, showing that the asynchronous excitation of the supports is not critical in this direction.

Figure 11 compares the peak demand for deformations in the H-LCP and Y-LCP models with $L_P = 400$ m when $\theta = 0°$. In the inverted 'Y'-shaped pylon the most critical region is the connection between the inclined legs and the top vertical member, where the maximum plastic strains reach 1.02% and 1.10% for the SVGM and the SYNC motions, respectively. This is explained by the connection between the inclined legs at this point which strongly constrains the pylon in the transverse direction. The connection between the legs and the strut, and the base of the pylon also represent critical sections where there is yielding of the steel in tension and softening of the concrete in compression. However, the peak plastic strains from the asynchronous excitations are smaller than the strains from the SYNC motion by $\rho_{\varepsilon_{tot}} = 0.57$ in the inverted 'Y'-shaped pylon. The stiff configuration of the inverted 'Y'-shaped pylon results in larger deformations at the critical sections compared to the 'H'-shaped pylon, as shown in Fig. 11, suggesting that the 'H'-shaped pylon is a better candidate to accommodate the seismic action in the range of intermediate spans with $L_P \approx 400$ m. This is in agreement with the elastic seismic analysis under SYNC motion conducted by Camara and Efthymiou [10] who observed that bridges with 'H'-shaped pylons are less sensitive to the transverse seismic reaction of the deck compared to bridges with inverted 'Y' pylons. However, the SVGM is not critical for the response of either pylon shapes when $\theta = 0°$.

3.4 Influence of the Pylon Height

Figure 12 presents the peak seismic response in terms of N, V_x and V_y in the pylons of the H-LCP models with $L_P = 200$, 400 and 600 m and $H_{tot} =$ 62.5, 125 and 187.5 m, respectively. It is observed that by increasing the main span length (L_P), the pylons are less vulnerable to the SVGM in terms of the vertical response, N. This is shown by the fact that the SVGM increases N in the relatively short pylon of the 200-m span bridge compared to the SYNC motion. Oppositely, both SVGM and SYNC motions result in similar values of N in the intermediate and tall pylons of the 400- and 600-m bridges, respectively.

The longitudinal response of the pylon is generally reduced by the SVGM regardless of the main span length which is reflected in the values of the response ratios; ρ_{V_x} ranges from 0.89 in the 200- and the 400-m span bridges to 0.86 in the 600-m span bridge. On the other hand, at the deck level of the pylon, increasing L_P has a considerable effect on the transverse response due to the SVGM. V_y is increased by the out-of-phase motion in the pylons of the 200- and the 600-m span bridges but is reduced when $L_P = 400$ m. The large seismic shear force in the pylon of the shortest bridge can be attributed to the stiffer configuration of this pylon compared to its longer counterparts when $L_P = 400$ or 600 m, given that stiff structures are reportedly vulnerable against the pseudo-static forces caused by the SVGM [37,41]. At the other end, the largest time-delay and loss of coherency in the 600-m span bridge combined with the increased height of the pylons and flexibility, result in pronounced transverse oscillations of the pylons and significant deck–pylon reactions. This explains the large V_y at the deck level of the pylon of the bridge with $L_P = 600$ m. Therefore, it is important to address the effect of the SVGM on the seismic response of the pylons not only on the basis of the length of the bridge, but also in terms of the pylons' height and geometric characteristics.

At the other end, the largest time-delay and loss of coherency in the 600-m span bridge combined with the increased height of the pylons and flexibility, result in pronounced transverse oscillations of the pylons and significant deck–pylon reactions. This explains the large Vy at the deck level of the pylon of the bridge with LP = 600 m

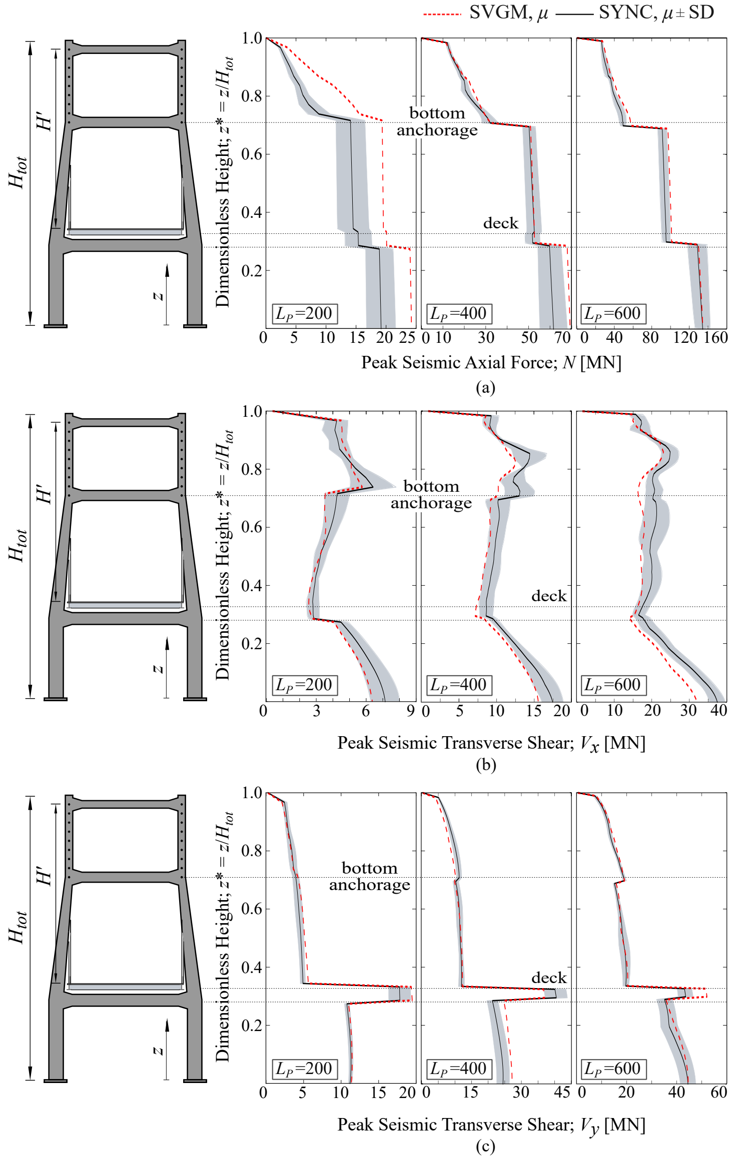

Fig. 12 Mean peak inelastic seismic (a) N, (b) V_x and (c) V_y along the height of pylon P2. H-LCP models; $\theta = 0°$ (i.e. FN // traffic).

Figure 13 presents the peak deformations in pylon P2 of the bridges with 200, 400 and 600 m main spans and 'H'-shaped pylons. With increasing main span length, the height of the pylon increases proportionally and it is observed that the peak deformations also increase in the connection between the legs and the upper strut. However, the short-span bridge (L_P = 200 m) is the one subjected to the largest demand of deformation at the region of the con-

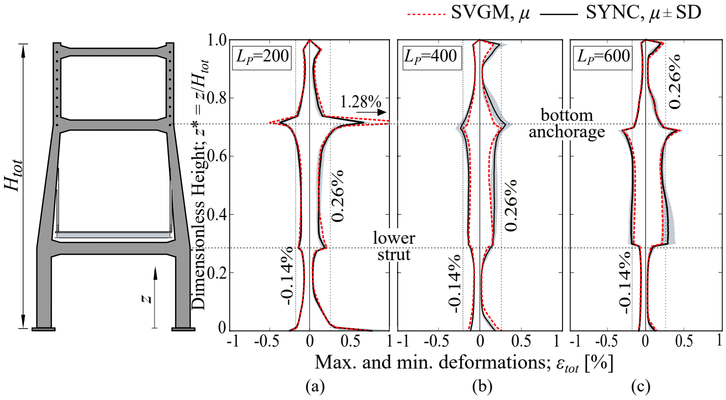

Fig. 13 Peak inelastic deformations of the concrete and the steel reinforcement in pylon P2 in the bridges with (a) $L_P = 200$ m, (b) $L_P = 400$ m and (c) $L_P = 600$ m. $\theta = 0°$. H-LCP models.

nection between the legs and the intermediate struts above the deck, whereas the reinforcement in the pylons of the 400-m span bridge barely exceeds its yielding point. The stiff pylon of the 200-m span bridge proves to be the most sensitive to the ground motion, especially under the SVGM, in which case the deformation ratio is $\rho_{\varepsilon_{tot}} = \frac{\varepsilon_{tot,\text{SVGM}}}{\varepsilon_{tot,\text{SYNC}}} = 2$. At the other end, the flexible pylon of the 600-m bridge is also susceptible to damage at the connection between the legs and the intermediate struts, but this is due to the relative transverse displacement between the legs that is accommodated by the struts. Furthermore, as the height of the pylon increases, the number of the cable anchorages increases proportionally, which adds to the vibration mass at the top of these structures and contributes to their relative displacement.

4 Conclusions

This paper examines the nonlinear response of cable-stayed bridges with different pylon shapes and span lengths under synchronous (SYNC) and asynchronous ground motions (SVGM) with different incidence angles. The seismic response of these bridges is discussed in terms of the peak seismic forces (N, V_x and V_y) and the deformations (ε_{tot}) that are developed in the pylons. The main conclusions drawn from this study are the following:

1. The shortest bridge ($L_P = 200$ m) is more sensitive to the SVGM than the intermediate- and long-span bridges with $L_P = 400$ and 600 m, respectively. The pylons of the 400-m span fall between the stiff pylons of the 200-m span bridge and the tall and flexible pylons of the 600-m span bridge. In the latter case the effect of the components of the SVGM (wave-passage and incoherence) are prominent because they are both functions of the separation distance between supports. These findings emphasise the

need for code-based provisions in which the importance of the SVGM for the design and assessment of bridges is established not only in terms of the total length but also in terms of the geometric characteristics of the structure.

2. The shape of the pylon influences the sensitivity to the asynchronous motion. The stiff configuration of the inverted ‘Y’-shaped pylon is more susceptible to the SVGM compared to the flexible ‘H’-shaped pylon. The most critical parts of the pylons are the connections between the legs and the transverse struts. The lateral flexure of the pylons is accommodated by the struts and the geometry that it conforms with the lateral legs.
3. The SVGM is detrimental to the transverse response of the pylons because in the this direction the pylon shape provides larger geometric stiffness than the one given by the constraint from the cable-system in the longitudinal direction. On the contrary, the longitudinal seismic response is consistently reduced by the multi-support excitation regardless of the height or the shape of the pylon, implying that the SVGM could potentially be neglected in this direction of the structural response.
4. The earthquake incidence angle with respect to the bridge (θ) is closely linked with the SVGM and with the response quantity under consideration. V_x, in the pylons is maximised when $\theta = 0°$ and the peak V_y is maximised when $\theta = 90°$, which is associated with the direction of the strong earthquake component. The wave-passage and incoherence effects are orientation dependent; therefore the effect of the SVGM is maximum when $\theta = 0°$.

Funding

This research did not receive any specific grant from funding agencies in the public, commercial, or not-for-profit sectors.

Conflict of interest

The authors declare that they have no conflict of interest.

Availability of data and material

Data sharing not applicable to this article as no datasets were generated or analysed during the current study.

References

1. Guide Specifications for LRFD Seismic Bridge Design - 2nd Edition (2011)
2. ABAQUS 2018. Finite elements analysis program; Providence, RI, Dassault Systèmes Simulia (2018)

3. Abdel-Ghaffar, A.: Cable - stayed bridges under seismic action. In: Cable - stayed Bridges; Recent Developments and their Future, pp. 171–192. Elsevier Science Ltd., Yokohama (Japan) (1991)
4. Abdel-Ghaffar, A., Nazmy, A.: 3D nonlinear seismic behavior of cable-stayed bridges. Journal of Structural Engineering **117**, 3456–3476 (1991)
5. Allam, S., Datta, T.: Seismic response of a cable-stayed bridge deck under multi-component non-stationary random ground motion. Earthquake Engineering & Structural Dynamics **33**, 375–393 (2004)
6. Bi, K., Hao, H., Ren, W.: Response of a frame structure on a canyon site to spatially varying ground motions. Structural Engineering and Mechanics **36**, 111–127 (2010)
7. Bruneau, M., Wilson, J.C., Tremblay, R.: Performance of steel bridges during the 1995 Hyogo-ken Nanbu (Kobe, Japan) earthquake. Canadian Journal of Civil Engineering **23**(3), 678–713 (1996)
8. Camara, A.: Seismic behaviour of cable-stayed bridges: Design, analysis and seismic devices. Ph.D. thesis, Universidad Politécnica de Madrid, Spain (2011)
9. Camara, A., Astiz, M., Ye, A.: Fundamental mode estimation for modern cable-stayed bridges considering the tower flexibility. Journal of Bridge Engineering **19** (2014)
10. Camara, A., Efthymiou, E.: Deck-tower interaction in the transverse seismic response of cable-stayed bridges and optimum configurations. Engineering Structures **124**, 494–506 (2016)
11. Chang, K.C., Mo, Y.L., Chen, C.C., Lai, L.A.C., Chou, C.C.: Lessons learned from the damaged Chi-Lu cable-stayed bridge. Journal of Bridge Engineering **9**(4), 343–352 (2004)
12. Deodatis, G.: Non-stationary stochastic vector processes: seismic ground motion applications. Probabilistic Engineering Mechanics **11**, 149–168 (1996)
13. Der Kiureghian, A.: A coherency model for spatially varying ground motions. Earthquake Engineering & Structural Dynamics **25**, 99–111 (1996)
14. Der Kiureghian, A., Neuenhofer, A.: Response spectrum method for multi support seismic excitations. Earthquake Engineering & Structural Dynamics **21**, 713–740 (1992)
15. Efthymiou, E.: The effect of multi-angle spatially variable ground motions on the seismic behaviour of cable-stayed bridges. Ph.D. thesis, City, University of London (2019)
16. Efthymiou, E., Camara, A.: Spatial variability effects of the seismic action in cable-stayed bridges and modelling techniques. In: IABSE Conference – Structural Engineering: Providing Solutions to Global Challenges. Geneva (Switzerland) (2015)
17. Efthymiou, E., Camara, A.: Effect of spatial variability of earthquakes on cable-stayed bridges. Procedia Engineering **199**, 2949–2954 (2017)
18. Efthymiou, E., Camara, A.: On the effect of multi-angle and spatially variable ground motions on cable-stayed bridges. engrXiv preprint (2020). DOI 10.31224/osf.io/4pufw
19. Eurocode 2: Design of concrete structures. Part 1.1: General rules and rules for buildings (2004). EN 1992-1-1:2004
20. Eurocode 3: Design of steel structures. Part 1.1: General rules and rules for buildings (2005). EN 1993-1-1:2005
21. Eurocode 3: Design of steel structures. Part 1.11: Design of structures with tension components (2006). EN 1993-1-11:2006
22. Eurocode 8: Design of structures for earthquake resistance. Part 1: General rules, seismic actions and rules for buildings (2004). EN 1998-1:2004
23. Eurocode 8: Design of structures for earthquake resistance. Part 2: Bridges (2005). EN 1998-2:2005
24. Filiatrault, A., Tinawi, R., Massicotte, B.: Damage to cable-stayed bridge during 1988 Saguenay earthquake. i: Pseudostatic analysis. Journal of Structural Engineering **119**(5), 1432–1449 (1993)
25. Gazetas, G.: Formulas and charts for impedances of surface and embedded foundations. Journal of Geotechnical Engineering **117**(9), 1363–1381 (1991)
26. Hao, H., Oliveira, C., Penzien, J.: Multiple-station ground motion processing and simulation based om SMART-1 array data. Nuclear Engineering and Design **111**, 293–310 (1989)
27. Harichandran, R., Vanmarcke, E.: Stochastic variation of earthquake ground motion in space and time. Journal of Engineering Mechanics **112**, 154–174 (1986)

28. HAZUS. Earthquake loss estimation methodology. Technical Manual (1997). HAZUS
29. Hilber, H., Hughes, T., Taylor, R.: Improved numerical dissipation for time integration algorithms in structural dymanics. Earthquake Engineering and Sructural Dynamics **5**, 283–292 (1977)
30. Hindy, A., Novak, M.: Pipeline response to random ground motion. Journal of the Engineering Mechanics Division **106**, 339–360 (1980)
31. Kawashima, K., Unjoh, S., Tunomoto, M.: Estimation of damping ratio of cable-stayed bridges for seismic design. Journal of Structural Engineering **119**(4), 1015–1031 (1993)
32. Khan, R.: Earthquake-Resistant Structures – Design, Assessment and Rehabilitation, chap. Seismic reliability analysis of cable-stayed bridges against first passage failure. INTECH Open Access Publisher (2012)
33. Lavorato, D., Fiorentino, G., Bergami, A.V., Briseghella, B., Nuti, C., Santini, S., Vanzi, I.: Asynchronous earthquake strong motion and RC bridges response. Journal of Traffic and Transportation Engineering (English Edition) **5**(6), 454–466 (2018)
34. Lopez, O., Hernandez, J., Bonilla, R., Fernandez, A.: Response spectra for multicomponent structural analysis. Earthquake Spectra **22**, 85–113 (2006)
35. Luco, J., Wong, H.: Response of a rigid foundation to a spatially random ground motion. Earthquake Engineering & Structural Dynamics **14**, 891–908 (1986)
36. Mander, J.B., Priestley, M.J.N., Park, R.: Theoretical stress-strain model for confined concrete. Journal of Structural Engineering **114**(8), 1804–1826 (1988)
37. Nazmy, A., Abdel-Ghaffar, A.: Effects of ground motion spatial variability on the response of cable-stayed bridges. Earthquake Engineering & Structural Dynamics **21**, 1–20 (1992)
38. Norma de Construcción Sismorresistente: Puentes (*in spanish*) (2007)
39. Nuti, C., Vanzi, I.: Influence of earthquake spatial variability on differential soil displacements and SDF system response. Earthquake Engineering & Structural Dynamics **34**(11), 1353–1374 (2005)
40. Priestley, M., Seible, F., Calvi, G.: Seismic design and retrofit of bridges. John Wiley & Sons Ltd. (1996)
41. Sextos, A., Kappos, A.: Asynchronous seismic excitation practice (*in greek*). In: 3^{rd} Panhellenic Conference on Earthquake Engineering and Engineering Seismology. Athens (Greece) (2008)
42. Sextos, A., Kappos, A., Mergos, P.: Effect of soil-structure interaction and spatial variability of ground motions on irregular bridges: The case of the Krystallopigi Bridge. In: 13^{th} World Conference on Earthquake Engineering. Vancouver (B.C. Canada) (2004)
43. Sextos, A., Karakostas, C., Lekidis, V., Papadopoulos, S.: Multiple support seismic excitation of the Evripos Bridge based on free-field and on-structure recordings. Structure and Infrastructure Engineering **11**, 1510–1523 (2014)
44. Sextos, A., Pitilakis, K., Kappos, A.: Inelastic dynamic analysis of RC bridges accounting for spatial variability of ground motion, site effects and soil–structure interaction phenomena. Part 1: Methodology and analytical tools. Earthquake Engineering & Structural Dynamics **32**(4), 607–627 (2003)
45. Shinozuka, M., Saxena, V., Deodatis, G.: Effect of spatial variation of ground on highway structures. Tech. rep., MCEER ISN 1520-295X (2000)
46. Soyluk, K., Dumanoglu, A.: Comparison of asynchronous and stochastic dynamic responses of a cable-stayed bridge. Engineering Structures **22**, 435–445 (2000)
47. Soyluk, K., Dumanoglu, A.: Spatial variability effects of ground motions on cable-stayed bridges. Soil Dynamics and Earthquake Engineering **24**, 241–250 (2004)
48. Stefanidou, S., Sextos, A., Kotsoglou, A., Lesgidis, N., Kappos, A.: Soil-structure interaction effects in analysis of seismic fragility of bridges using an intensity-based ground motion selection procedure. Engineering Structures **151**, 366–380 (2017)
49. Tzanetos, N., Elnashai, A., Hamdan, F., Antoniou, S.: Inelastic dynamic response of RC bridges subjected to spatial non-synchronous earthquake motion. Advances in Structural Engineering **3**, 191–214 (2000)
50. Wang, J., Carr, A., Cooke, N., Moss, P.: Wave-passage effect on the seismic response of long bridges. In: 2003 Pacific Conference on Earthquake Engineering (2003)
51. Zerva, A.: Effect of spatial variability and propagation of seismic ground motions on the response of multiply supported structures. Probabilistic Engineering Mechanics **6**, 212–221 (1991)

52. Zerva, A.: Spatial variation of seismic ground motions: Modeling and engineering applications. CRC Press, Boca Raton (2009)